Graphene-based plastic absorber for total sub-terahertz radiation shielding†

Mariusz Zdrojek, [ID] *[a] Jarosław Bomba,[a] Anna Łapińska,[a] Anna Dużyńska,[a] Klaudia Żerańska-Chudek,[a] Jarosław Suszek,[a] Leszek Stobiński,[b] Andrzej Taube, [ID] [a,c] Maciej Sypek[a] and Jarosław Judek [ID] [a]

Increasing the requirements on telecommunications systems such as the need for higher data rates and connectivity *via* the Internet of things results in continuously increasing amounts of electromagnetic radiation in ever-higher telecommunications bands (up to terahertz). This can generate unwanted electromagnetic radiation that can affect the operation of electronic devices and human health. Here, we demonstrate that nonconductive and lightweight, graphene-based composites can shield more than 99.99% of the electromagnetic energy in the sub-THz range mainly *via* absorption. This contrasts with state-of-the-art electromagnetic radiation shielding materials that simply redirect the energy of the radiation from a protected area *via* conduction-based reflection mechanisms. This shifts the problem of electromagnetic pollution from one place to another. We have demonstrated that the proposed composites can be fabricated by industrial compatible methods and are characterized by specific shielding efficiency values that exceed 30 dB cm³ g⁻¹, which is more than those for typical metals used today. Therefore these materials might help to solve the problem of electromagnetic environmental pollution.

Introduction

Terahertz electromagnetic radiation is usually defined in the frequency range of 0.1–10 THz, has huge and growing potential in many different fields such as *e.g.* telecommunications, security, fast sensing and imaging, and medicine.[1–6] This is possible due to the rapid development of the construction of emitters and detectors operating in the sub-terahertz and terahertz part of the spectrum.[7] Future telecommunication and electronics need to shift to THz technology to meet the growing demand for ultra-fast wireless data transfer systems and new functionalities. Accordingly, the space around us will be increasingly filled with electromagnetic waves (EM) in this range and a substantial increase in unwanted electromagnetic pollution in the environment will become a problem if no shielding is provided. This is because sub-terahertz and terahertz radiation can impact sensitive electronic devices leading to their malfunctioning, which can also affect living organisms or human health.[5,8–10] Therefore, effective attenuation – most preferably *via* absorption of electromagnetic radiation – is a key aspect for the further development of terahertz technology.

Today, conventional state-of-the-art materials that protect against terahertz are metals (*e.g.* aluminum, copper) or metal-based conducting coatings and composites. These materials shield electromagnetic radiation across a wide range of the spectrum including the microwave (gigahertz) range. However, the shielding mechanism is based on the interaction of the free carriers in the conductive metallic material with incoming EM waves resulting in reflection. This leaves unwanted radiation still in the surrounding environment. Another drawback of using a metal-based shield is that it cannot always be easily applied as an electrically conductive material; it has low plasticity and high specific weight. It is also not compatible with current manufacturing technologies, *e.g.* molding. An alternative approach is to use polymer-based materials with metallic or nanostructures fillers that can exhibit effective electromagnetic interference (EMI) shielding properties in the GHz range[11–13] while also possessing useful functionalities (*e.g.* flexibility, light weight).

The above shielding technologies mostly use reflection. Generally speaking, studies on the shielding properties in the sub-terahertz and terahertz range are still in their initial stage, and only a few examples have been demonstrated thus far. Recently, most attention has been focused on polymer-based composites with nanocarbon fillers (nanotubes, nanofibers,

[a]Faculty of Physics, Warsaw University of Technology, Koszykowa 75, 00-662 Warsaw, Poland. E-mail: mariusz.zdrojek@pw.edu.pl
[b]Faculty of Chemical and Process Engineering, Warsaw University of Technology, Warynskiego 1, 00-645 Warsaw, Poland
[c]Institute of Microelectronics and Optoelectronics, Warsaw University of Technology, Koszykowa 75, 00-662 Warsaw, Poland

†Electronic supplementary information (ESI) available: Details of calculation of SE parameters in THz regime, additional data presenting reflectance spectra measurements, THz EMI shielding demonstration on video and Fig. S1–S5. See DOI: 10.1039/c8nr02793e

and nanographite)[14–20] or large-scale graphene multilayer sandwiches.[21–23] For example, the carbon nanotubes/polyvinyl ether (PVE) composite films are reported to exhibit shielding efficiency (SE) exceeding 10 dB (in 0.3–2.1 THz range)[14] while superhydrophobic composite based on polymer (PTFE) filled with carbon nanowhiskers[15] exhibit a shielding effectiveness of ~40 dB in 0.57–0.63 THz range, showing that the shielding mechanism is based on reflection (similarly as for metals). Additionally, the graphite-based composites have been demonstrated to be excellent shielding material,[18,20] with SE exceeding 30 dB (with high graphite loading, >10%). Graphene has been also considered as THz absorber due to its broadband and strong interaction with electromagnetic waves. Several works on terahertz transmittance or attenuation level through single and few layer graphene films have been reported,[21–23] for instance showing SE as high as 16 dB at 1.2 THz for five graphene/dielectric layer stack,[21] while for monolayer graphene the attenuation is only ~1 dB. However, until now, composite with graphene flakes as a THz shielding material has been not demonstrated. Despite numerous efforts, no real breakthrough results have been achieved.[24] This is because the proposed materials offer satisfactory shielding performance *via* distribution of the filler in the polymer host to create a macroscopic network making the composite electrically conductive. They thus still exhibit metal-like shielding functionality based mostly on reflection.
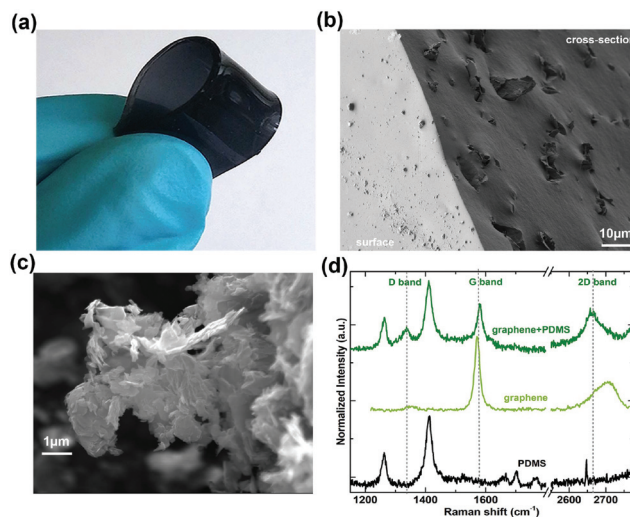
The ideal sub-terahertz and terahertz shield should not only protect the selected component from the radiation but also reduce this radiation in the environment *via* its efficient absorption. Flexible and lightweight features are equally desirable, *e.g.* for the protection of flexible electronics[25] or movable electronics parts. In addition, it is useful that the shielding material not be electrically conductive to prevent electrical short-cuts. This is crucial for the protection of electronic components. All these imply a need for new materials that can replace metal-like shielding materials and reduce EM pollution while also reducing weight, decreasing costs, and increasing corrosion resistance/flexibility.

Here we demonstrate a flexible and lightweight nanocomposite material that attenuates radiation in the sub-terahertz range while also being electrically non-conductive. The nanocomposite is based on graphene flakes dispersed in an elastomer matrix fabricated through a simple solution mixing method. Its EMI shielding effectiveness is high enough to block ~99.99% of the radiation at a graphene loading level of 10 wt%. Importantly, we demonstrate that the main mechanism responsible for high shielding efficiency is the absorption. The reflection is relatively low unlike the common shielding materials used today. In addition, the material is transparent to microwaves.

Experimental methods

Sample fabrication

The graphene/polidimethylosiloxane (PDMS) nanocomposites were fabricated using the polidimethylosiloxane purchased

Fig. 1 The structural characterization and shielding properties of composite in sub-THz range. (a) A photograph demonstrating the flexibility (1 wt% graphene) of the composite material. (b) SEM image of cross-section of the composite showing flakes immersed in a polymer matrix. (c) SEM of a graphene flakes used for composite production. (d) Raman spectra of PDMS and graphene/PDMS composite (10 wt%) showing the evidence of graphene presence (D, G, and 2D bands).

from Dow Corning (SYLGARD 184) and graphene nanopowder (Fig. 1(c)) with the lateral particle size of ~10 microns and thickness of up to 10 nm (Graphene Supermarket, grade C1). The procedure of sample fabrication was as follows. The appropriate amount of PDMS base was mixed with appropriate amount of graphene nanopowder (mechanical mixing). The volume of graphene nanopowder was adjusted to the needed concentration of final product (we used weight concentration: 0.1%, 3%, and 10%). The mixture of graphene and base PDMS was placed in an ultrasonic bath (Elmasonic) and remained there for 2 hours at a frequency of 80 kHz and 100% power with additional pulse mode (power up to 20% due to enforcement of peak performance). The temperature was held low during the sonication process. Afterwards, the curing agent was added to the pre-composite at a rate of 1 : 10. The material was mixed vigorously for a couple of minutes and then poured to the final matrix. To remove the air bubbles that appeared during the mixing process, the composite was placed in a desiccator and held in a vacuum for 1 hour. To speed up the curing process, the composite was heated up to 100 °C for 1 hour in the oven.

Raman spectroscopy

The Raman spectra of pristine graphene powder, PDMS, and graphene/PDMS composites (Fig. 1(c)) were collected using a Renishaw inVia Raman spectrometer with λ_{ex} = 633 nm laser line excitation and 50× lens (NA = 0.5). Measurements were conducted at room temperature using low laser power (<1 mW).

Electrical conductivity (DC)

Transport measurements were performed using a Keithley 2450 Source Measurement Unit, National Instrument NI

USB-6366 Data Acquisition Card, DL1211 current preamplifier, and Keithely 7065 Hall Effect Card connected to Signatone probe station. Typical measurement schemes include two-probe measurements, four-probe measurements, and measurements using the Van der Pauw technique.

Time domain spectroscopy setup and raw data processing

The THz pump–probe measurement procedure is as follows. The emitter and detector (low-temperature-grown GaAs (LT-GaAs) photoconductive (PC) antenna) are illuminated by a femtosecond laser (fs) in typical pump and probe setup using low power density of few $\mu W\ cm^{-2}$. A mechanical delay line was used to change the time delay between THz pulse and the probe pulse (signal is detected when optical paths are equal). Importantly, the optical setup was goniometric for expanding the detection area to detect both the specular and diffusive reflection/transmission effects. The optical beam is delivered to the detector *via* an optical fiber, and the shape of the beam is divergent. The size of the beam at the surface of the sample is about 3 cm. The beam polarization is parallel to the goniometric setup plane. The detector moves on a circle with a radius of 20 cm. The measurement is fully automatic *via* a stepper line motor in delay line. The stepper rotary motor is in the detection part. We used this setup for transmission (Fig. S2B†) and reflection measurement modes (Fig. S2A†). In transmission mode, the flat sample is mounted perpendicular to the THz beam. The range of the measured angle was ±15 degrees from the center of the beam with 1 degree sampling. In reflection mode, the sample was mounted at several angles to the beam. The range of the measured angle was ±15 degrees from the center of reflected beam, with 1 degree sampling.

Measuring signal in time-domain (Fig. S3A†) gives amplitude with a wide spectrum of frequency range (100 GHz to 1 THz) after Fourier Transform (Fig. S3B†). The signals collected at a ±15 degree range generate a spatial plot (Fig. S3C†). Finally, at each frequency, the signal is averaged over the degree range, *i.e.* the amplitude values are summed and divided by the number of the samples. The transmitted and reflected signals are divided by the reference signal recorded simultaneously.

The EMI shielding in GHz regime

For the measurements of electromagnetic shielding effectiveness, we used a technique based on the ASTM D4935-99 standard developed by the American Society for Testing and Materials (ASTM) in 1999 using an enlarged coaxial transmission and network analyzer (Agilent N5241A) that measures the S matrix parameters. The vector analyzer output gives S_{21} that is related to the GHz radiation transmittance/shielding efficiency as: $T = |S_{21}|^2$.

Results and discussion

The three different graphene contents (0.1, 3, and 10 wt%) have been used to produce composites (~0.6 mm thick, flex-

ible, and soft 10 cm diameter dicks). They are opaque to visible light for graphene flake concentrations larger than 1 wt% (see Fig. S1†). The density of the composite with the highest graphene concentration is ~1.1 g cm^{-3}.

Fig. 1(a) shows a typical fabricated graphene/polydimethylsiloxane (PDMS) composite sample that was used for transmittance and reflectance measurements. As a starting point of the as-prepared composites characterization scanning electron microscope imaging (SEM), Raman spectroscopy and DC electrical study has been employed, showing morphology and structural properties (Fig. 1(b–d)).
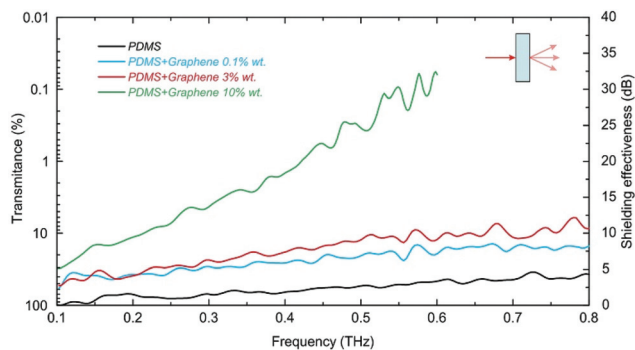
In the spectra of graphene/PDMS composites (Fig. 1(d)) and theirs components, several peaks originating from the PDMS matrix are visible: ~1260 cm^{-1} and 1410 cm^{-1} originating from CH$_3$ symmetrical and antisymmetrical bending, respectively.[26] The bands located at 1570 cm^{-1} and 2700 cm^{-1} are assigned to the G and 2D bands and confirm the presence of graphene in the polymer matrix. There is also a small intensity peak at 1350 cm^{-1} that is assigned to the D band, associated with disordered structure of graphene. The I(D)/I(G) ratio was low at 0.33 showing that the graphene properties were not affected by the composite fabrication process, as the I(D)/I(G) for graphene powder was ~0.1. Also, the Raman spectra are not affected by the change of graphene loading.

The DC electrical measurements showed that the transport properties of the graphene-PDMS composite are the same as pure PDMS (see Fig. S5†). This clearly indicates that no macroscopic percolation conducting network was formed even with high graphene loads (10%). This is also confirmed by SEM images of the composite cross-section, shown in Fig. 1(b). As can be seen, the graphene sheets (SEM image of raw material is shown in Fig. 1(c)) are randomly distributed in PDMS matrix, however, they tend to agglomerate and wrinkle, and there is no visible connection between them. Thus, in our case the composite is bellow percolation threshold. Within all THz shielding materials, only our graphene-PDMS composite is non-conductive. To validate EMI shielding properties of our composites in sub-THz range, the transmittance and reflectance spectra using the THz-TDS method[27] were measured including a specular/diffusive detection approach (see Fig. S2C†).

Fig. 2 presents the measured transmittance in the sub-THz range (0.1–0.8 THz) for bare PDMS and graphene/PDMS composites with different graphene contents (0.1, 3 and 10 wt%). The transmittance of the reference sample and the graphene-enriched composites are gradually decreasing with increasing frequency. More importantly, they decrease with graphene load. For composites with a graphene loading of 10 wt%, the transmittance at 0.1 THz is already at 30%. This rapidly decreases with frequency to ~0.01% at 0.6 THz (see Fig. 2, green curve). For higher frequencies, the signal is lower than the noise level of our detection system.

Based on transmittance measurements, the shielding effectiveness (SE) on the dB scale was calculated using expression SE(dB) $= -10 \log_{10}(T)$ where T is measured transmittance. The corresponding SE spectra in the sub-THz range are depicted in
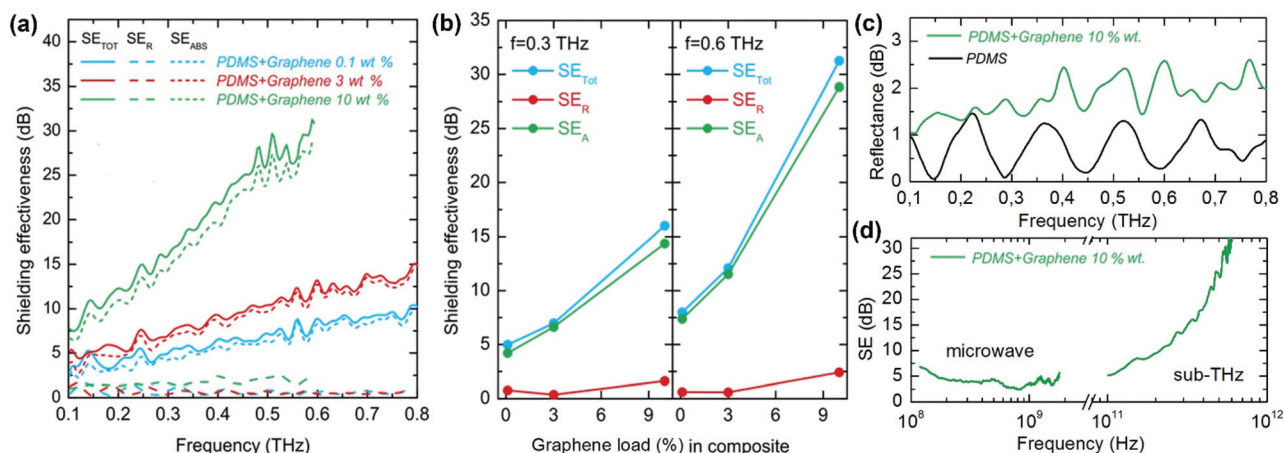
Fig. 2 The transmittance spectra and EMI shielding effectiveness of composites with different graphene contents measured from 0.1–0.8 THz. (See the movie file (S1†) for life demonstration of the shielding effect). Top-right schematic shows transmission model indicating measurement of specular and diffusive radiation. We note that THz wave is not depolarized within the sample.

Fig. 2 (scale on the right). As can be seen, the SE of the pristine polymer is rather poor, (~4 dB at 0.8 THz), in contrast to the SE of the graphene composites. The shielding efficiency of the composites with 0.1 and 3 wt% graphene is ~2.5 dB at 0.1 THz, which increases up to ~10 dB at 0.8 THz. The SE parameter for the composite with the highest graphene load of 10 wt% is ~5 dB at 0.1 THz. This rapidly elevates and reaches ~34 dB at 0.6 THz. This value is much more than is needed for commercial applications, which usually require more than 20 dB. Another criterion for validation of the shielding performance compared with other existing materials is the specific shielding effectiveness (SE divided by the material density). A 10 wt% graphene load could reach ~31 dB cm^3 g^{-1} at 0.6 THz. This value is significantly higher than those of common metals (10 dB cm^3 g^{-1}) for bulk copper[27] or other conductive nanocarbon-based solid structure composites[15,24] suggesting

that our composites are good candidates as a lightweight high-performance shielding material[28] for portable electronics, aerospace, or automotive applications.

We further analyzed the possible THz shielding mechanisms of the graphene-based composites by determining whether the reflection or absorption is the key factor standing behind the SE parameter. The absorbance (A) strictly depends on reflectance (R) and transmittance (T), i.e. the amount of the wave intensity that penetrates and crosses the material is $1 - R$ and $(1 - R)(1 - A)$, respectively. Thus measuring the T and R allows one to discriminate the different contributions of these mechanisms to SE.

Both reflectance and transmittance were measured in the configuration where the incident electromagnetic wave was at 45° angle (Fig. S2C†). In this case, the total shielding effectiveness (SE$_{TOT}$) is the sum of absorption (SE$_{ABS}$) and reflection (SE$_R$) i.e. SE$_{TOT}$ = SE$_{ABS}$ + SE$_R$ neglecting the contribution of multiple reflections (justified by the condition that the incident wavelength is longer or comparable to the composite thickness). The SE$_{ABS}$ can be expressed and calculated as SE$_{ABS}$ = $-10 \log_{10}(T/(1 - R))$. Fig. 3(a) shows all components: SE$_{TOT}$ (solid lines), SE$_R$ (long dash lines), and SE$_{ABS}$ (short dash lines). These were measured for graphene/PDMS composites with respect to the graphene load level. Importantly, these results show that the main contribution to the total shielding effectiveness for our composites is the absorption. Moreover, the SE$_R$ is at the same and relatively low level over all studied frequencies. The SE$_R$ oscillates around 1–2 dB and slightly increases with frequency for 10 wt% graphene load sample (see more details in ESI†). Fig. 3(b) compares the contribution of attenuation mechanisms at 0.3 THz and 0.6 THz. The contribution of absorption increases with graphene load much faster than the reflection. The SE$_{ABS}$ at 0.3 THz increases up to ~15 dB as the graphene load increases to 10%; for 0.6 THz, the SE$_{ABS}$ increases from 6.2 dB to ~26 dB.

Fig. 3 The EMI shielding mechanisms and broadband properties of the composite (a) comparison of contribution of radiation attenuation mechanism to total shielding effectiveness graphene/PDMS composites measured at incident angles of 45° as shown in S2C.† (b) Comparison of shielding mechanism at f = 0.3 THz and 0.6 THz for different graphene loads. (c) The reflectance spectra measured at 45° incidence angle for bare polymer and composite sample (10% graphene loading). (d) Microwave shielding effectiveness of graphene-based composite (10 wt%) measured in the UHF and L band (0.2–1.8 GHz) compared with the SE for sub-THz from Fig. 2.

We note that the absorptive character of EMI shielding mechanism of our composites is significantly different from those of metals,[27] CNT/graphite based composites,[17,19,24] or graphene or in graphene (for very high optical conductivity)[22] where reflection is the main contribution to EMI shielding due to the interaction of EM wave with free carriers (model in Fig. 4). The unique SE properties of our composite can be understood *via* several following mechanisms. The low reflection level is because our composite carriers are restricted only to the separated graphene flakes that are randomly immersed in the polymer matrix (Fig. 4). This makes the entire material nonconductive. This causes the reflection mechanism to not be effective. On the other hand, the architecture of the composite implies conditions where the electrons (in graphene) behave more like bonded charges.[19] This generates a polarization-like contribution to the attenuation of THz waves that is extremely high. Another important mechanism is related to the interaction of atomic vibration (active in infrared/THz range) in disordered material and inter-band transitions (π-band to polaron band) that are in resonance with THz radiation producing its massive absorption.[20,27,29] The multiple internal reflection/absorption mechanism is much less probable because the wavelength of incident radiation is much bigger than the flake size.

We also found that our graphene composites can act as a low pass filter for electromagnetic radiation because they are an effective shield against sub-THz radiation that shows transparency at microwave UHF (300 MHz–1 GHz) and L (1–2 GHz) bands. The average values in the SE in the microwave range is only about 4 dB as shown in Fig. 2(d) (the measurement procedure is described in the ESI†). This finding contrasts with other works where graphene/nanocarbon-based foams or composites[11,30,31] usually show excellent SE performances in this range. In our case, the low value of SE in the microwave range stems from the lack of macroscopic percolation networks in our material. This suppresses the main shielding mechanism in the GHz range, *i.e.*, scattering on free carriers.
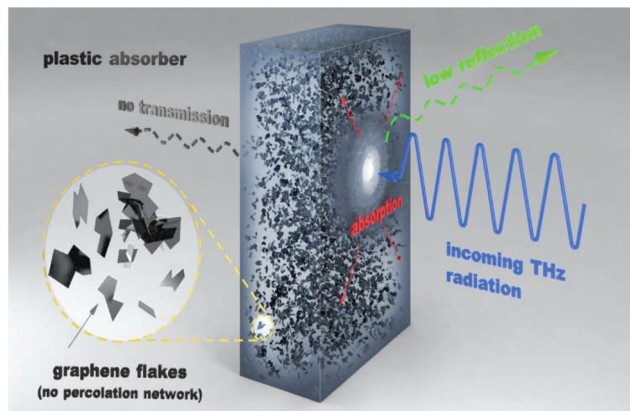

Fig. 4 Proposed mechanisms of interaction of THz wave with graphene based composite.

Conclusions

In summary, we synthetized and characterized the first non-conductive, lightweight, and flexible graphene-based composites with the unique capacity for efficient sub-THz shielding based mainly on absorption in contrast to most well-known metal-like materials that operate based on reflection. Our materials pave the way toward efficient elimination of unwanted/parasitic THz radiation from the environment. In the future, these materials may be further improved by better control of material architecture (*e.g.* different matrix, other 2D materials as fillers) with a goal to tune the shielding efficiency and attenuation mechanisms. We believe that the proposed material together with further improvements can solve the dramatic increase in the electromagnetic pollution of the environment (electromagnetic smog) while also meeting the requirements of future terahertz electronics, imaging, and telecommunications systems.

Conflicts of interest

The authors declare that have no competing and financial interest.

Acknowledgements

Notes and references

1 T. Nagatsuma, G. Ducournau and C. C. Renaud, *Nat. Photonics*, 2016, **10**, 371–379.

2 M. Tonouchi, *Nat. Photonics*, 2007, **1**, 97–105.

3 J. F. Federici, B. Schulkin, F. Huang, D. Gary, R. Barat, F. Oliveira and D. Zimdars, *Semicond. Sci. Technol.*, 2005, **20**, S266–S280.

4 H.-J. Song and T. Nagatsuma, *IEEE Trans. Terahertz Sci. Technol.*, 2011, **1**, 256–263.

5 L. Zhao, Y.-H. Hao and R.-Y. Peng, *Mil. Med. Res.*, 2014, **1**, 26.

6 R. I. Stantchev, B. Sun, S. M. Hornett, P. A. Hobson, G. M. Gibson, M. J. Padgett and E. Hendry, *Sci. Adv.*, 2016, **2**, e1600190–e1600190.

7 M. Lee and M. C. Wanke, *Science*, 2007, **316**, 64–65.

8 T. Kleine-Ostmann, C. Jastrow, K. Baaske, B. Heinen, M. Schwerdtfeger, U. Karst, H. Hintzsche, H. Stopper, M. Koch and T. Schrader, *IEEE Trans. Terahertz Sci. Technol.*, 2014, **4**, 12–25.

9 A. Ramundo Orlando and G. P. Gallerano, *J. Infrared, Millimeter, Terahertz Waves*, 2009, **30**(12), 1308–1318.

10 B. S. Alexandrov, K. Ø. Rasmussen, A. R. Bishop, A. Usheva, L. B. Alexandrov, S. Chong, Y. Dagon, L. G. Booshehri, C. H. Mielke, M. L. Phipps, J. S. Martinez, H.-T. Chen and G. Rodriguez, *Biomed. Opt. Express*, 2011, **2**, 2679–2689.

11 F. Shahzad, M. Alhabeb, C. B. Hatter, B. Anasori, S. M. Hong, C. M. Koo and Y. Gogotsi, *Science*, 2016, **353**, 1137–1140.

12 T.-W. Lee, S.-E. Lee and Y. G. Jeong, *ACS Appl. Mater. Interfaces*, 2016, **8**, 13123–13132.

13 X. Shui and D. D. L. Chung, *J. Electron. Mater.*, 1997, **26**, 928–934.

14 D. Polley, A. Barman and R. K. Mitra, *Opt. Lett.*, 2014, **39**, 1541.

15 A. Das, T. M. Schutzius, C. M. Megaridis, S. Subhechha, T. Wang and L. Liu, *Appl. Phys. Lett.*, 2012, **101**, 243108.

16 J. T. Hong, D. J. Park, J. Y. Moon, S. B. Choi, J. K. Park, F. Rotermund, J.-Y. Park, S. Lee and Y. H. Ahn, *Appl. Phys. Express*, 2012, **5**, 15102.

17 M. A. Seo, J. H. Yim, Y. H. Ahn, F. Rotermund, D. S. Kim, S. Lee and H. Lim, *Appl. Phys. Lett.*, 2008, **93**, 231905.

18 M. A. Seo, J. W. Lee and D. S. Kim, *J. Appl. Phys.*, 2006, **99**, 66103.

19 L. Ren, C. L. Pint, L. G. Booshehri, W. D. Rice, X. Wang, D. J. Hilton, K. Takeya, I. Kawayama, M. Tonouchi, R. H. Hauge and J. Kono, *Nano Lett.*, 2009, **9**, 2610–2613.

20 P. Chamorro-Posada, J. Vázquez-Cabo, Ó. Rubiños-López, J. Martín-Gil, S. Hernández-Navarro, P. Martín-Ramos, F. M. Sánchez-Arévalo, A. V. Tamashausky, C. Merino-Sánchez and R. C. Dante, *Carbon*, 2016, **98**, 484–490.

21 H. Yan, X. Li, B. Chandra, G. Tulevski, Y. Wu, M. Freitag, W. Zhu, P. Avouris and F. Xia, *Nat. Nanotechnol.*, 2012, **7**, 330–334.

22 B. Sensale-Rodriguez, R. Yan, M. M. Kelly, T. Fang, K. Tahy, W. S. Hwang, D. Jena, L. Liu and H. G. Xing, *Nat. Commun.*, 2012, **3**, 780.

23 J. M. Dawlaty, S. Shivaraman, J. Strait, P. George, M. Chandrashekhar, F. Rana, M. G. Spencer, D. Veksler and Y. Chen, *Appl. Phys. Lett.*, 2008, **93**, 131905.

24 L. Liu, A. Das and C. M. Megaridis, *Carbon*, 2014, **69**, 1–16.

25 J. A. Rogers, T. Someya and Y. Huang, *Science*, 2010, **327**, 1603–1607.

26 D. Cai, A. Neyer, R. Kuckuk and H. M. Heise, *J. Mol. Struct.*, 2010, **976**, 274–281.

27 J. Lloyd-Hughes and T.-I. Jeon, *J. Infrared, Millimeter, Terahertz Waves*, 2012, **33**, 871–925.

28 Z. Chen, C. Xu, C. Ma, W. Ren and H.-M. Cheng, *Adv. Mater.*, 2013, **25**, 1296–1300.

29 S. N. Taraskin, S. I. Simdyankin, S. R. Elliott, J. R. Neilson and T. Lo, *Phys. Rev. Lett.*, 2006, **97**, 55504.

30 B. Shen, W. Zhai and W. Zheng, *Adv. Funct. Mater.*, 2014, **24**, 4542–4548.

31 D.-X. Yan, P.-G. Ren, H. Pang, Q. Fu, M.-B. Yang and Z.-M. Li, *J. Mater. Chem.*, 2012, **22**, 18772.